Electrochimica Acta 252 (2017) 523–531

Contents lists available at ScienceDirect

Electrochimica Acta

journal homepage: www.elsevier.com/locate/electacta

Research paper

Highly Reversible Sodium-ion Storage in $NaTi_2(PO_4)_3$/C Composite Nanofibers

Min Li[b], Li Liu[a,b,d,*], Peiqi Wang[c], Jiangyu Li[c], Qianyi Leng[b], Guozhong Cao[a,*]

[a] Materials Science Engineering, University of Washington, WA 98105, Seattle, USA
[b] International Science and Technology Cooperation Base of New Energy Equipment and Energy Storage Materials, Xiangtan University, Xiangtan 411105, Hunan, China
[c] Mechanical Engineering, University of Washington, WA 98105, Seattle, USA
[d] Key Laboratory of Advanced Energy Materials Chemistry (Ministry of Education), Nankai University, Tianjin 300071, China

ARTICLE INFO

Article history:
Received 14 April 2017
Received in revised form 4 September 2017
Accepted 4 September 2017
Available online 6 September 2017

Keywords:
Sodium titanium phosphate
sodium ion batteries
electrospinning
nanofibers

ABSTRACT

$NaTi_2(PO_4)_3$/C composite nanofibers (NTP/C-F)have been prepared with success by electrospinning followed by calcination in Ar. For comparison, $NaTi_2(PO_4)_3$ nanofibers have also been synthesized by similar method but calcination in air. $NaTi_2(PO_4)_3$/C composite particles without special morphology also have been prepared by directly calcining the precursor in Ar. The samples have been characterized by scanning electron microscopy (SEM), High-resolution transmission electron microscopy (HRTEM), X-ray diffraction (XRD), X-ray photoelectron spectroscopy (XPS), charge-discharge test, cyclic voltammetry (CV), electrochemical impedance spectroscopy (EIS). NTP/C-F demonstrates excellent sodium ion storage properties including good rate capability and extended cycle life, much better than other two samples. It delivers the highest discharge capacities, which are about 130, 123, 122, 119, 114, 103, 87, and 63 mAh g^{-1} at 0.1, 0.2, 0.5, 1, 2, 5, 10, and 20 C, respectively. The discharge capacity reserves as high as 97 mAh g^{-1} after 500 cycles at 5 C, and the corresponding capacity retention is 93%. Such outstanding property is likely due to the special 1D-structure including uniform electrically conductive carbon network, which brings high electronic conductivity and rapid Na^+ diffusion. Hence, NTP/C-F will be a potential electrode candidate for sodium ion batteries.

1. Introduction

Nowadays, in different portable electronics, high energy lithium ion batteries have been extensively used as power sources for applications. However, their applications ingrid-scale energy storage, such as electric vehicles and smart grids, have been seriously hindered because of their high cost, mainly due to the limited lithium mineral reserves and growing price of lithium commodity chemicals. As alternative, sodium ion batteries (SIBs), which is good candidates, are considered for large-scale energy storage applications and have drawn increasing attention in the past few years owing to their low-cost and earth-abundant sources [1–5]. Naturally, in order to get suitable electrode materials for sodium ion batteries, significant efforts have been devoted, but SIB technology still remains in its infancy, and the electrode materials with high cyclability and rate performance are being developed.

In sodium ion batteries, NASICON (Na^+ superionic conductor)-type sodium titanium phosphate ($NaTi_2(PO_4)_3$) has arousing a significant interest as an electrode. Its three-dimensional framework possess highly covalent and super sodium ion conducting structure offer a 3 D sodium ion intercalation pathway, which result in its clearly defined redox potential (2.1 V vs. Na^+/Na) with two Na ions intercalation/deintercalation, delivering a theoretical specific capacity of 133 mAh g^{-1} [6]. However, the defect, mainly including those 3-D phosphates with the quite low intrinsic electronic conductivity [7–9], have prevented $NaTi_2(PO_4)_3$ from being far and widely used in large-scale applications. Numerous researchers have confirmed that nanostructure of the active material as well as the addition of conductive agents, such as carbon, is a hopeful strategy for preparing high-property electrode materials. There were two methods usually adopted for that purpose. The first method is to use carbon matrix with special 3D, 2D or porous structure to host $NaTi_2(PO_4)_3$ nanoparticles, such as using a mesoporous carbon (CMK-3) and graphene as matrices to

* Corresponding authors at: Materials Science Engineering, University of Washington, WA 98105, Seattle, USA.
E-mail addresses: liulili1203@126.com (L. Liu), gzcao@u.washington.edu (G. Cao).

http://dx.doi.org/10.1016/j.electacta.2017.09.020
0013-4686/

prepare $NaTi_2(PO_4)_3$/CMK-3 and $NaTi_2(PO_4)_3$/graphene nanocomposites respectively by solvothermal methods [10,11]. Zhao et al. synthesized hollow carbon spheres first and used them as a matrix to fabricate porous $NaTi_2(PO_4)_3$–C array [12]. The second method is to prepare $NaTi_2(PO_4)_3$ nanostructures and then apply in-situ carbon coating. Difi et al. synthesized Fe-doped $NaTi_2(PO_4)_3$ by a solid-state method and then used sucrose as carbon sources to prepare Fe-doped $NaTi_2(PO_4)_3$/C composite [13]. In the previous work, we synthesized $NaTi_2(PO_4)_3$ porous plates via a solvothermal approach and utilized carbonization of glucose to obtain $NaTi_2(PO_4)_3$/C porous plates with good electrochemical properties [14]. These methods undoubtedly prepared $NaTi_2(PO_4)_3$/C composites with improved performance successfully, while these methods are relative complicated. The contact between $NaTi_2(PO_4)_3$ particles and carbon in these products is less ideal, thus the improvements of electronic conductivity and electrochemical performance are limited.

Besides the formation of composite with carbon, the fabrication of 1D nanostructure is another effective and interesting approach to improve the electrochemical performance of electrode materials for sodium ion batteries. The previous many reports indicated the significance of one-dimensional (1D) nanostructure, such as nanotubes, nanowires, nanofibers and nanobelts, as functional materials for potential applications in plenty of areas. To serve as electrode materials for sodium ion batteries, there are many advantages for 1D nanostructure materials; for instance, shortened Na-ion insertion/extraction distance, facile strain relaxation upon electrochemical cycling, and large surface to volume ratio, resulting in enhancing capacity and cyclicity of sodium ion batteries. Although many synthetic approaches for preparing $NaTi_2(PO_4)_3$/C composites have been reported, as far as we know, the $NaTi_2(PO_4)_3$/C composites with 1D nanostructure have not been reported yet because of the lack of appropriate and generalized synthetic methodologies. However, it is noteworthy that the electrospinning technique is widely used to fabricate ultrafine hierarchical 1D nanostructure with controllable diameters, aspect ratios, compositions, directions and constructions, and it is a common method to fabricate many electrode materials for lithium ion batteries. Recently, we have successfully synthesized other titanium-based electrode materials with 1D nanostructure, such as $LiTi_2(PO_4)_3$/C nanofibers, using electrospinning technique and the improved electrochemical performance has been obtained [15]. Electrospinning provided a more simple and effective process to synthesize $LiTi_2(PO_4)_3$/C composites. Obviously, it is a workable way to combine 1 D nanostructure and carbon composite to greatly enhance the electrochemical property of electrode materials [16–19].

This paper reports electrospinning is first used to fabricate one-dimensional (1D) $NaTi_2(PO_4)_3$/C composite nanofibers. The electrospun $NaTi_2(PO_4)_3$/C composite nanofibers were found to offer excellent rate capability and cycling stability. Vast characterizations were implemented for the electrospun $NaTi_2(PO_4)_3$/C nanofibers and electrochemical performances were assessed by the way of half-cell configuration with different testing conditions. The relationships between the composition, crystallinity, morphology including nano- and microstructures, and the sodium ion storage properties have been elaborated.

2. Experimental

2.1. Preparation of Materials

The precursor solution for electrospinning was synthesized by dissolving 0.274 g of phosphorous pentoxide (P_2O_5, Aldrich, purity 98%), 0.1239 g of sodium propionate (CH_3CH_2COONa, Aldrich, purity 99.95%), 0.7355 g of Titanium (IV) isopropoxide ($C_{12}H_{28}O_4Ti$, Aldrich, purity 97%), and 0.15 g of polyvinylpyrrolidone (PVP, Mw = 1300000, Alfa-Aesar) in 5 ml ethanol at about 50 °C by stirring for 12 hours, then forming the viscous pale yellow clear solution. A 10 mL syringe connected by a blunt-tip stainless-steel needle is used to load the precursor solution. The flow rate of the solution was 0.5 mL h^{-1} controlled by a syringe pump (NE-300, New Era Pump System, Inc., USA). The metallic needle was connected to a high voltage power supply (ES30, Gamma High Voltage Research, Inc, USA). A grounded alumina foil, which was 20 cm away from the tip of needle, was used as collector for precursor fibers. A voltage of 20 kV was applied to start the electrpspinning. In Ar at 750 °C,the as-collected precursor fibers were calcined for 6 h to gain $NaTi_2(PO_4)_3$/C nanofibers composite (named as NTP/C-F). Fig.S1 shows a schematic diagram of the experimental procedure.

For comparison, bare $NaTi_2(PO_4)_3$ nanofibers (named as bare NTP) were prepared by calcination of the electrospun precusor fibers in air at 750 °C for 6 h. Besides, the $NaTi_2(PO_4)_3$/C composite particles (named as NTP/C-P) were acquired by immediate calcination of precusor solution in uniform conditions followed by grinding.

2.2. Structure Characterization and Electrochemical Measurements

The precursor and products was analyzed by thermogravimetry (TG) by means of a Thermogravimetric–differential Thermal analyzer (TGAQ50, TA instruments).X-ray diffraction spectroscopy (XRD) is used to characterize the structures of prepared samples. X-ray powder diffraction data were obtained by a Rigaku D/MAX-2500 powder diffractometer with a graphite monochromatic and Cu Kα radiation (λ=0.15418 nm) in the 2θ range of 10–80°.

A JEOL SM-71480 scanning electron microscope was used to collect scanning electron microscope (SEM) images of the sample. High-resolution transmission electron microscopy (HRTEM) and selected-area electron diffraction (SAED) measurements were executed, which use a JEOL JEM-2100F transmission electron microscope at an acceleration voltage of 200 kV. And X-ray photoelectron spectroscopy (XPS ESCALAB 250 Xi Thermo Fisher Scientific, America) was performed to examine the composition of surface materials. The active materials, carbon black, and polyvinylidene fluoride (PVDF) binder of a weight ratio of 70:20:10 are mixed, in order to fabricate the cathodes for sodium cells. Generally, the mass of the positive active material is about 1.3 mg per electrode and the area of per electrode is about 0.785 cm^2. So electrode density is around 1.66 mg cm^{-2}.The cathodes thus fabricated, metallic sodium anode, glass fiber separator (Whatman GF/A) and 1 M $NaClO_4$ in 1:1 propylene carbonate (PC)/ethylene carbonate (EC) electrolyte including 5 wt% of fluoroethylene carbonate (FEC) assemble the testing cells. An argon-filled glove box is used to assemble the testing cells, where concentrations of water and oxygen were kept less than 1 ppm. The discharge–charge cycle tests were run at various current densities between 3.3 and 1.5 V. All the tests were carried out at room temperature.

Both cyclic voltammetry (CV) tests and EIS experiments were performed on a CHI604E potentiostats-electrochemistry workstation. CV tests were executed at the various scan rates on the potential interval 1.5–3.3 V (vs. Na^+/Na). The signal of ac perturbation was ±5 mV, and the frequency range was 100 mHz–10^5 Hz.

3. Results and discussion

3.1. Structure and morphology

Fig. 1a displays the thermogravimetric (TG) curves of the precursor fibers gained over the temperature range from 30 to

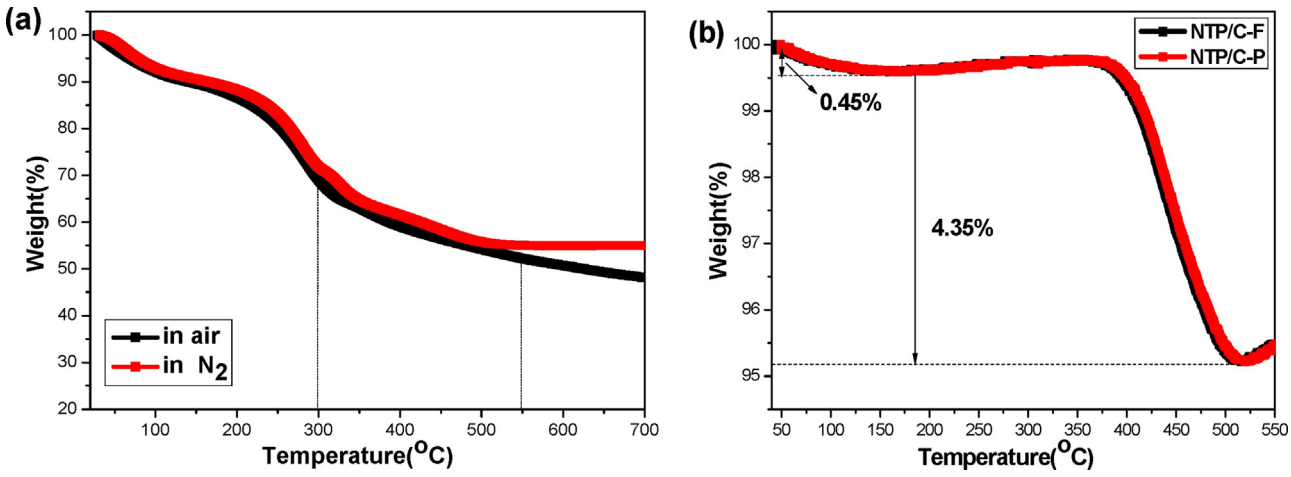

Fig. 1. TG curves of the precursor recorded from 30 to 700 °C at the heating rate of 10 °C min^{-1} in N_2 and air (a); TG curves of NTP/C-F and NTP/C-P from 50 to 550 °Cat the heating rate of 10 °C min^{-1} in air (b).

700 °C in the atmosphere of air and N_2. There are two obvious regions of weight loss in the regions of 30–300 °C and 300–550 °C. The precursor fibers show almost the same trend in the first weight loss region (30–300 °C) in two different gases. The weight loss is around 30%, which is primarily due to the release of ethanol and the decomposition of sodium acetate and titanium (IV) isopropoxide. The second steep weight loss, which takes place between 300 and 550 °C, mainly arises from the decomposition of PVP and the formation of $NaTi_2(PO_4)_3$. However, the precursor fibers show much different weight losses in different gases at temperatures higher than 550 °C. The weight losses are about 49% in air and 45% in N_2, respectively. The difference of weight loss (around 4%) can be due to that PVP can be decomposed completely in air, while a certain amount of carbon exists when PVP decomposes in N_2. So the carbon amount in NTP/C-F and NTP/C-P materials is proposed to be approximately 4%. To further estimate the content of carbon in the NTP/C-F and NTP/C-P, TG analysis was carried out in air. It is observed that NTP/C-F and NTP/C-P show similar TG curves (see Fig. 1b).These two samples demonstrate a weight loss of about 0.45% and 4.35% in the regions of 50–100 °C and 100–520 °C, respectively. Before 100 °C is due to the evaporation of adsorbed water, and a weight loss of about 4% in the regions of 400-520 °Cis attributable tocontent of organic carbon. Hence, the approximate amount of carbon in NTP/C-F and NTP/C-P is calculated to be about 4 wt%, which is accorded with the results of Fig. 1a.

Fig. 2 shows the XRD patterns of bare NTP, NTP/C-P and NTP/C-F. Almost all reflections in these samples could be indexed on the basis of a rhombohedral $NaTi_2(PO_4)_3$ structure with a space group of R3c (JCPDS: 84-2009). A little impurity phase of $Ti_2O(PO_4)_2$ was detected in these patterns, which could be attributed to the impurities from H_3PO_4 (reacted reagents P_2O_5) and products TiO_2. No detectable reflections corresponding to graphite was observed in the XRD patterns of NTP/C-P and NTP/C-F on account of its low content and amorphous nature. To further confirm the structure of NTP/C-F, the XPS survey of NTP/C-F is shown in Fig. S2.

Fig. 3 displays SEM images of the precursor nanofibers, NTP/C-F, bare NTP, and NTP/C-P. The precursor nanofibers have a smooth surface (see Fig. 3a). Close observation (see the inset in Fig. 3a) reveals that the nanofibers show diameters of 100–200 nm. After annealing in Ar, the continuous 1D nanostructure was retained, but a notable change occurred in the surface and length of nanofibers. The surface of NTP/C-F is rough, and the annealing also shortens the fibers (see Fig. 3b). Bare NTP shows shorter length than that of NTP/C-F (see Fig. 3c), and this may be due to the absence of carbon in bare NTP cause the poor tenacity of fibers. The diameters of bare NTP and NTP/C-F are similar to precursor nanofibers, which are in the range of 100–200 nm. According to reports, active materials with one-dimensional (1D) nanostructure have both nano-size merits: (1) Na-ion diffusion pathway is shorter; (2) when self-aggregation is limited, facile strain relaxation and large surface to volume ratios to contact with the electrolyte. Fig. 3d presents SEM images of NTP/C-P, which shows that the NTP/C-P is composed of nonuniform micron-sized particles.

The morphology of NTP/C-F can be further observed by TEM as shown in Fig. 4a. NTP/C-F shows nanofibers with diameters within 200 nm, which are identical with the results of SEM image (see Fig. 3a). Besides, it seems that NTP/C-F is composed of NTP primary nanoparticles with diameter below 10 nm and carbon matrix. The HRTEM image of NTP/C-F is given in Fig. 4b, which shows NTP/C-F crystallites consist of amorphous carbon region and the lattice fringes. The lattice fringes are corresponding to the (202) and (024) d-spaces of NTP.As identified in Fig. 4c, The SAED pattern of NTP/C-F shows that five ring patterns related to (1115), (137), (119), (300) and (202) planes and broad ring patterns exist simultaneously, and the indices accord with rhombohedra NTP/C-F. This is also in accordance with the XRD results (shown in Fig. 2). To further identify the structure of NTP/C-F, NTP/C-F composites were annealed in air at 750 °Cfor 2 h to remove the carbon matrix and treated in HF solution to remove the NTP primary

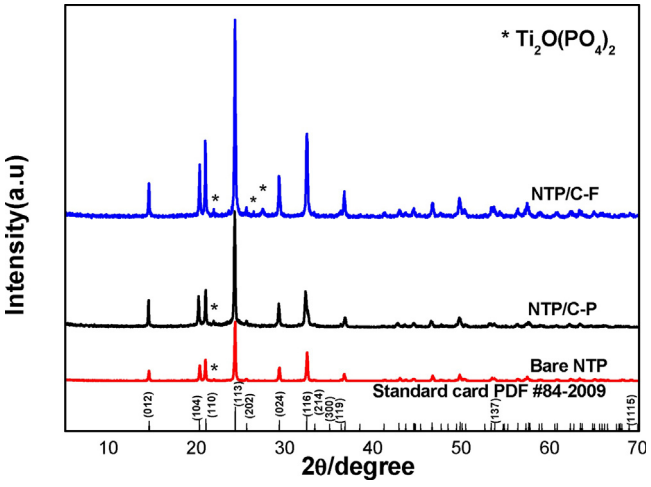

Fig. 2. XRD patterns of bare NTP, NTP/C-P and NTP/C-F.

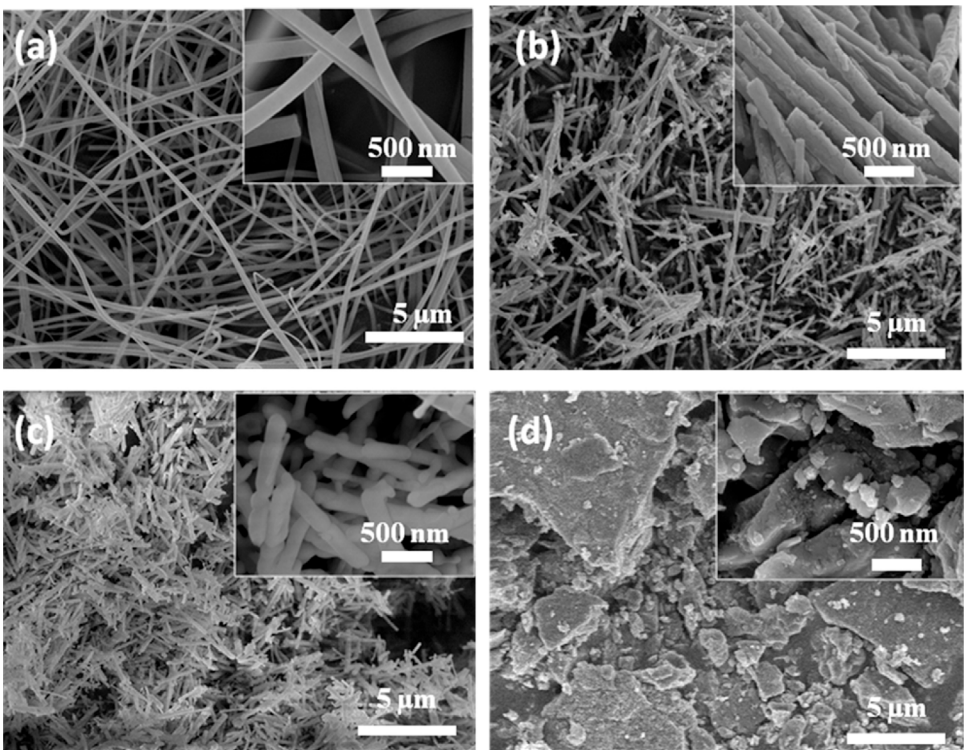

Fig. 3. SEM images electrospun nanofibers before annealing (a), NTP/C-F (b), bare NTP (c) and NTP/C-P (d).

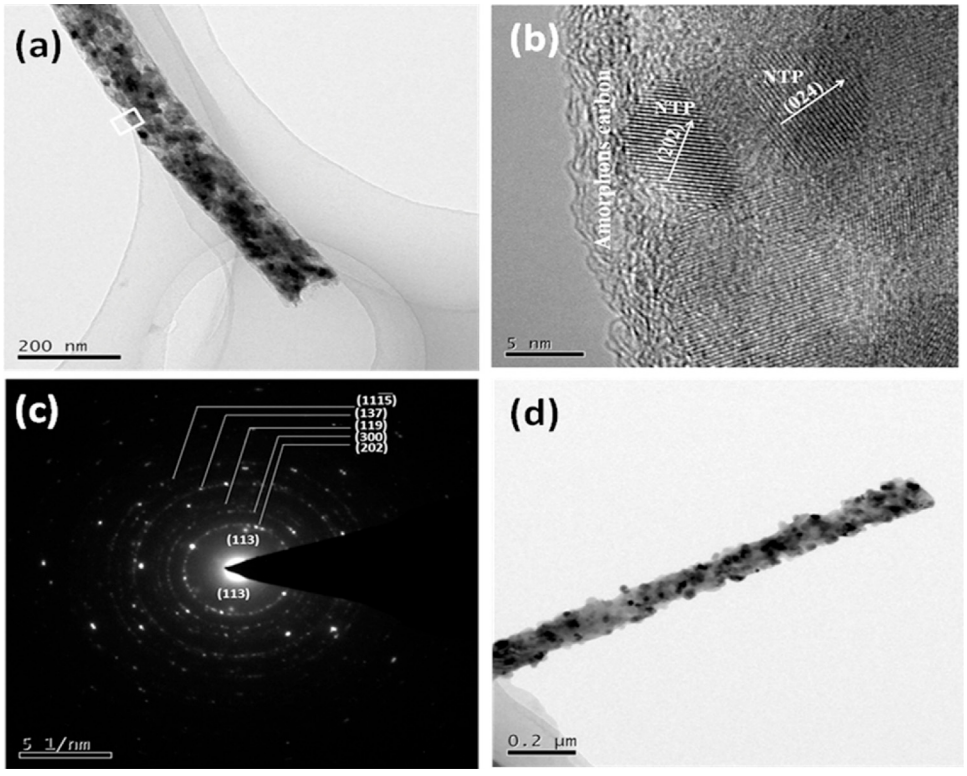

Fig. 4. TEM (a), HRTEM (b) images, and SAED pattern (c) of NTP/C-F; TEM image of the sample formed by annealing NTP/C-F in air at 750 °C for 2 h (d).

nanoparticles, respectively, and their TEM images are shown in Fig. 4d and Fig. S3. After annealing in air, NTP primary nanoparticles with diameter below 10 nm could be clearly observed (see Fig. 4d). Additional, residual 1D carbon matrix could be clearly detected after treatment with HF solution (see Fig. S3). NTP primary nanoparticles provides very short Na-ion and electron diffusion pathway. Besides, the 1D carbon matrix form good electro-conductive network, which can interconnect the $NaTi_2(PO_4)_3$primarynanoparticles, hence the sites where redox reactions take place can readily transmit the electrons.

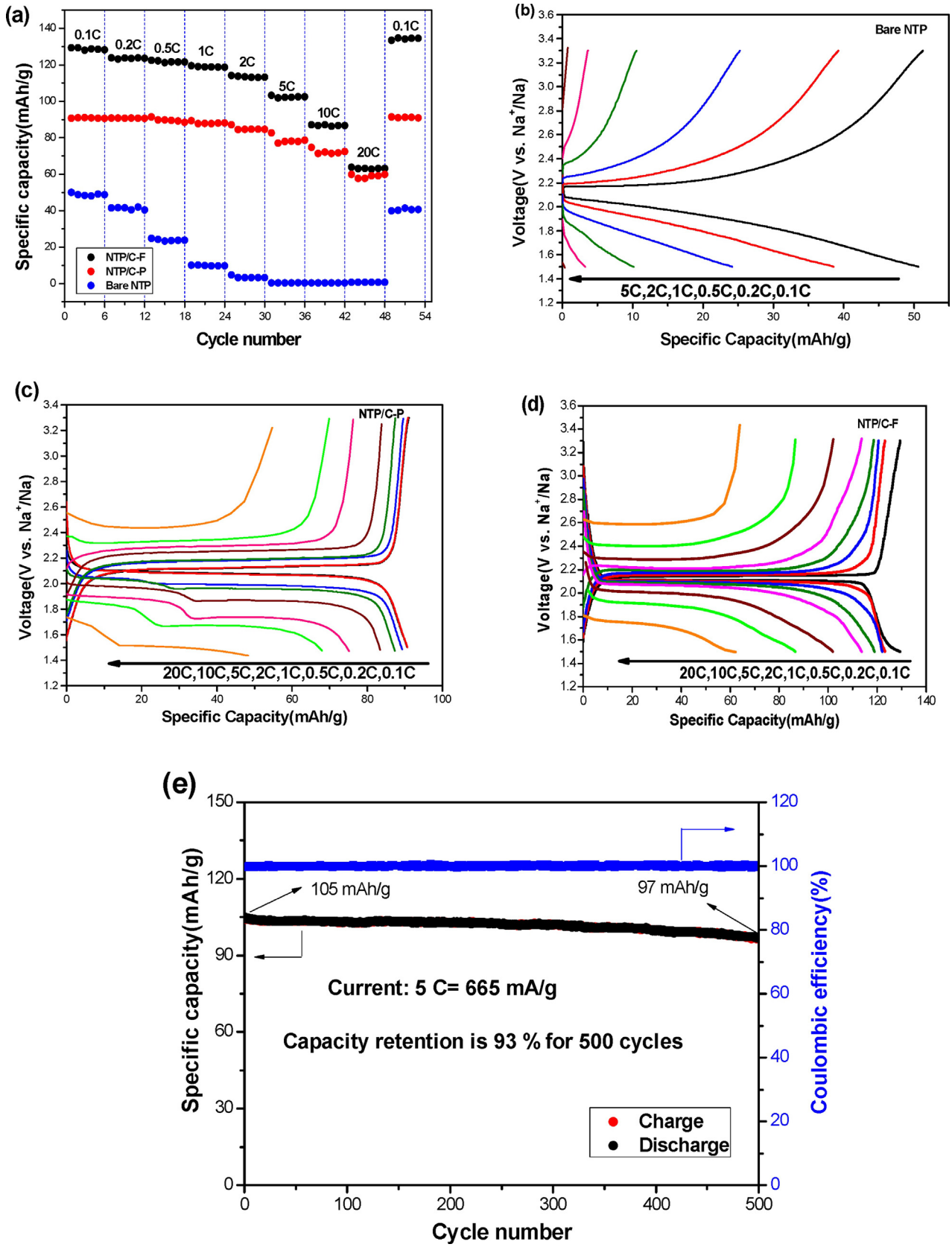

Fig. 5. Discharge capacity retention data of NTP/C-F, NTP/C-P and bare NTP for successive cycling at different rates (a); the corresponding discharge and charge profiles of bare NTP (b), NTP/C-P (c), NTP/C-F at different rates (d).discharge/charge capacity as a function of cycle number of NTP/C-F at 5 C (e).

3.2. Electrochemical studies

To well know the rate capability during the charge/discharge process, the specific discharge capacities of NTP/C-F, NTP/C-P and bare NTP at different discharge/charge rates ranging from 0.1 C (1C = 133 mAh g^{-1}) to 20 C have been tested (see Fig. 5a). At the current density of 0.1 C, the first discharge capacities of NTP/C-F, NTP/C-P and bare NTP are 129, 91, and 50 mAh g^{-1}, respectively. Bare NTP not only shows low specific capacity, but also shows very poor rate capability. At the current densities of 0.5 C and 1 C, it delivers discharge capacities of about 40 and 23 mAh g^{-1}, respectively. With the current density above 2 C, it delivers very low specific capacities, which are below 10 mAh g^{-1}. Although bare NTP has 1 D nanofibers structure, it shows a very poor electrochemical performance. This may be due to the large primary particles and poor electronic conductivity when absence of carbon. NTP/C-P shows much better rate capability than bare NTP. With the current density increasing from 0.1 C to 1 C, the discharge capacity hardly decreases.At the current densities of 0.2 C, 0.5 C and 1 C, it delivers discharge capacities of about 90, 89 and 88 mAh g^{-1}, respectively. Furthermore, the discharge capacities only decrease to 70 and 60 mAh g^{-1} at very high current densities of 10C and 20C, respectively. When it is tested at a low current density of 0.1C again, the capacity can return to about 90 mAh g^{-1}. So it is obvious that NTP/C-P is in the nature of better rate capability. Among these samples, NTP/C-F delivers the highest discharge capacities, which are about 130, 123, 122, 119, 114, and 103 mAh g^{-1} at the current densities of 0.1 C, 0.2 C, 0.5 C, 1 C, 2 C, and 5 C, respectively. It even can deliver discharge capacities as high as about 87 and 63 mAh g^{-1} at very high current densities of 10 C and 20 C, respectively. After such high current density test, the reversible capacity can still recover to about 130 mAh g^{-1} at 0.1 C. Although NTP/C-P also shows excellent rate capability, its specific capacity is much lower than that of NTP/C-F. As we mentioned, the NTP/C-F possess the best electrochemical performance. The excellent electrochemical properties of NTP/C-F could be attributed to its special 1D-structure with small nanosized NTP primary particles and uniform electrically conductive carbon network. The 1D-structure provides the high electro-active surface area, which offers an enhanced contact between active material and electrolyte so the electron transport gets improved. Additional, small nanosized NTP primary particles are in favor of Na^+ and electron diffusions. Moreover, the formation of uniform electrically conductive carbon network further increase electronic conductivity, reduce cell polarization, and stabilize the structure of active materials. Fig. 5b illustrates the discharge/charge evolution of bare NTP from 0.1 to 5 C. With the current density constantly increasing, the specific capacity quickly decreasing and is below 10 at 5C due to its low electron conductivity. And the discharge/charge evolution of NTP/C-P and NTP/C-F are shown in Fig. 5c, d. There are the typical voltage plateau in the discharge–charge profiles for NTP/C-P and NTP/C-F, which attributed to the two-phase reaction of the $NaTi_2(PO_4)_3$ and $Na_3Ti_2(PO_4)_3$ system. And at a slow rate of 0.1 C, there is a plateau at about 2.1 V vs. Na^+/Na in the discharge curves, which is consistent with the reaction $NaTi_2(PO_4)_3 + xNa^+ + xe^- \rightarrow Na_{1+x}Ti_2(PO_4)_3$. However, at higher current rates, NTP/C-P displays an additional discharge plateau located at around 2.0 V. That is due to local heating induced by higher charge/discharge rates, resulting in Na^+ can occupy two different sites and migrate easily between each other in the NASICON NTP framework [20,21]. Obviously, with the current density constantly increasing and the specific capacity gradually decreasing, the charge/discharge polarization becomes more and more apparent for NTP/C-P and NTP/C-F.

To further show the electrochemical behavior of NTP/C-F, cycle performance of NTP/C-F at 5C are illustrated in Fig. 5e, which demonstrates excellent capacity retention of NTP/C-F with coulombic efficiency near 100%. The discharge capacity of NTP/C-F at the first cycle is 105 mAh g^{-1}, and it reserves as high as 97 mAh g^{-1} after 500 cycles. The capacity decay is only 7% after 500 cycles. For all we know, such excellent high-rate property and cycle performance are superior to most of existing electrode materials reported for sodium ion batteries. Indubitably, the electrochemical performance of NTP/C-F is much better than most of the other previously reported $NaTi_2(PO_4)_3$ based materials.

Table 1 compares some previous research results on $NaTi_2(PO_4)_3$/C composites synthesis and their electrochemical properties with the results of our study .It can be seen that electrospun NTP/C-Fin this work displays higher specific capacity and better cyclability than NTP/CMK-3 and NTP/C prepared by solvothermal methods [10,14]. Greatly benefited from the unique properties of graphene, NTP/graphene composites showed excellent rate capability [22–24]. It is obvious that the rate capability of electrospun NTP/C-F is comparable with NTP/grapheme prepared by a sol-gel method [22]. Although electrospun NTP/C-F shows lower specific capacity than NTP/rGO (reduced grapheneoxide) and the NTP/graphene prepared by a solvothermal method at 20 C [23,24], its cyclability is better than the NTP/rGO and is comparable with the NTP/graphene. It is note that although NTP/graphene composites showed outstanding electrochemical performance, the synthesis processes were complicated. The graphene should be carefully prepared in advance, and the full contact between NTP particles and graphene needs be guaranteed. Therefore, electrospun NTP/C-F in present work is one of active materials with great promise for the application of sodium-ion battery.

Fig. 6a compares the cyclic voltammograms of bare NTP, NTP/C-P and NTP/C-F. Bare NTP shows a pair of redox peaks located at 1.99 V and 2.27 V. The redox peaks of NTP/C-P and NTP/C-F are

Table 1
Comparison on electrochemical performances of $NaTi_2(PO_4)_3$/C composites prepared by various methods.

Synthesis Method (ref)	Composition	Voltage range (V)	Current Density	Capacity (mA g^{-1}) (cycle number)	Capacity Retention
solvothermal method [10]	NTP/CMK-3	1.0-3.0	0.5C	74.5(200)-62.9(1000)	–
solvothermal method [14]	NTP/C	1.5-3.3	700 mA·g^{-1}	95 (1)-82(120)	0.86
sol-gel method [20]	NTP/graphene	1.5-3.8	100mA·g^{-1}	121(1)-102(700)	0.84
			5C	100.3(1)	
			10C	87.9(1)	
			20C	63.5(1)	
polyol-assistedpyro–synthesis [21]	NTP/rGO	1.0-3.0	1C	117.6(1)-100(150)	0.85
			20C	91(1)-62(1000)	0.68
hydrothermal method [22]	NTP/graphene	1.5-3.0	10C	96 (1)- 83(500)	0.86
			20C	~85	
Present work: Electrospinning	NTP/C	1.5-3.3	5C	104.5 (1)-96.7(500)	0.93
			10C	~87	
			20C	~63	

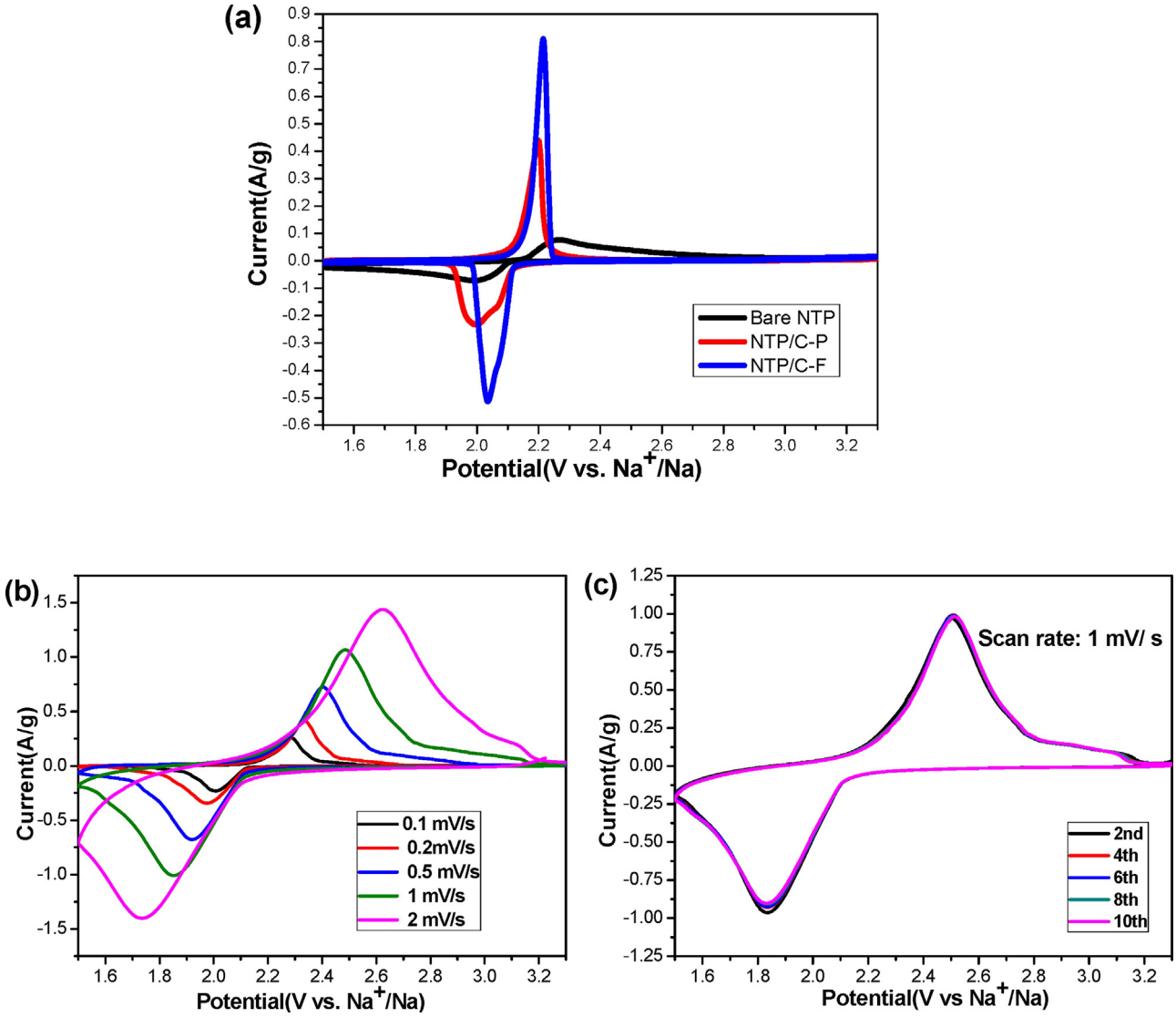

Fig. 6. Cyclic voltammograms of bare NTP, NTP/C-P and NTP/C-F for the second cycle (a) (scan rate is 0.1 mV·s^{-1}); cyclic voltammograms of NTP/C-F at different scan rates(b) and at a scan rate of 1 mV s^{-1}in various cycles(c).

located at 1.98/2.20 V and 2.03/2.21 V,respectively. This pair of redox peaks are the typical redox peaks of $NaTi_2(PO_4)_3$. The insertion/removal of Na into/from the $NaTi_2(PO_4)_3$ and $Na_3Ti_2(PO_4)_3$ structure are characterized by the peak observed in the cathodic sweep and the anodic sweep [25], which can be correlated with Ti^{4+}/Ti^{3+} redox reaction. However, there are other unconspicuous reductive peaks appear to be located at 2.072 V for NTP/C-P and 2.069 V for NTP/C-F, which is attributed to the activation in the first cycle [26]. It is noteworthy that the CV curves have no double reductive peaks for NTP/C-F at the scan rate of 1 mV s^{-1} in Fig. 6(c). The reason is the shapes of peak could not be clearly and completely showed at higher scan rate. The difference of voltage between the anodic and the cathodic peaks reflects the degree of polarization of the electrode. A serious polarization behavior is indicated by the potential difference between the anodic and cathodic peaks (ΔEp = 0.28 V) of bare NTP, which is attributed to the quite limited electrical conductivity of the $NaTi_2(PO_4)_3$. The value of ΔEp (0.22 V) of NTP/C-P is much lower than that of bare NTP, indicating the weaker polarization with better reversibility of the electrode. But NTP/C-F displays the lowest value of ΔEp (0.18 V), showing its best electrochemical reversibility.

The CV curves of NTP/C-F at various scan rates ranging from 0.1 to 2 mV s^{-1} are shown in Fig. 6b. As scan rate increases, the anodic peak voltage shifts to higher value, while that of the cathodic peak voltage moves to lower voltage value. It is on account of polarization. Nevertheless, when the scan rate adds to 2 mV s^{-1}, the peaks retain the well-defined shape, revealing the good reversibility of the charge/discharge reaction. Fig. 6c shows cyclic voltammogram of NTP/C-F at a scan rate of 1 mV s^{-1}in various cycles. It is found that the peak current densities are nearly changeless and the curves are almost identical upon cycling, indicating NTP/C-F displays outstanding cycle performance and reversibility. It is in good agreement with the long term cycling stability of NTP/C-F displayed in Fig. 5c.

The Nyquist plots of bare NTP, NTP/C-P and NTP/C-F are illustrated in Fig. 7a. An intercept at the Z' axis of the high frequency indicates the ohmic resistance (R_Ω) [27], which represents the resistance of the electrolyte and electrode material. The charge transfer resistance (R_{ct}) is characterized by the semicircle in the middle frequency range [28,29]. The inclined line of the low frequency represents the Warburg impedance (W), which is related to the diffusion of sodium ions in the solid matrix. The impedance spectra have been analyzed by constructed a

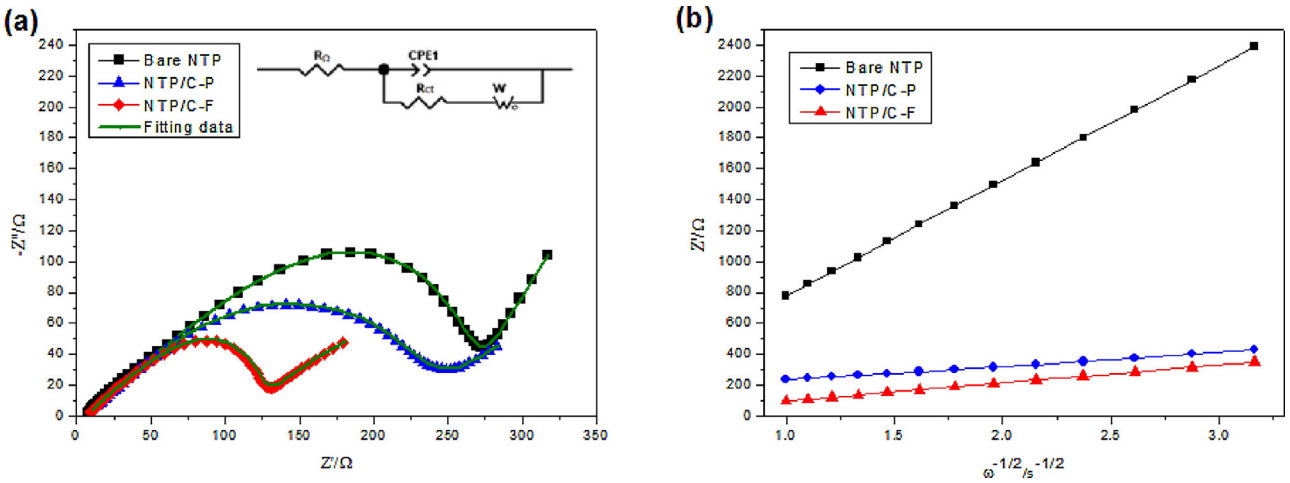

Fig. 7. Nyquist plots of bare NTP, NTP/C-P and NTP/C-F (the inset is the equivalent circuit model) (a); the linear relationship plot between Z' and $\omega^{1/2}$ at low frequency region (b).

Table 2
Kinetic parameters for bare NTP, NTP/C-P and NTP/C-F.

Samples	R_{Ω} (Ω)	R_{ct} (Ω)	D_{Na+} ($cm^2 s^{-1}$)
Bare NTP	9.557	235.8	2.91×10^{-13}
NTP/C-P	8.822	180.3	4.26×10^{-10}
NTP/C- F	6.606	78.8	7.42×10^{-10}

simplified equivalent circuit model (see the inset of Fig. 7a). A constant phase element *CPE* is placed to represent the double layer capacitance and passive film capacitance [30,31]. The parameters of the equivalent circuit are recorded in Table 2. It is clear that the R_{Ω} of NTP/C-F is 6.606 Ω, which is smaller than that of bare NTP or NTP/C-P. Moreover, the R_{ct} of NTP/C-F is 78.8 Ω, which is smaller than that of NTP/C-P and much smaller than that of bare NTP. Hence, it can be deduced that NTP/C-F displays the smallest electrochemical resistance, indicating its best electron conductivity and electrochemical activity. The electronic conductivity of NTP/C-F measured by the four point probe tester is 1.447×10^{-2} S cm^{-1}, and it is higher than NTP/C-P (1.023×10^{-2} S cm^{-1}) and bare NTP (1.031×10^{-4} S cm^{-1}). So it shows the best electrochemical properties.

The diffusion coefficient of sodium ion (D_{Na+}) can be calculated from the sloping line according to the following equations [32,33]:

$$D_{Na^+} = \frac{R^2T^2}{2A^2n^4F^4C^2\sigma_w^2} \quad (1)$$

$$Z' = Rs + Rct + \sigma_w\omega^{-1/2} \quad (2)$$

where R is the gas constant, T is the absolute temperature, A is the surface area of the cathode, n is the number of electrons per molecule during oxidization, F is the Faraday constant, C is the concentration of sodium ion, σ_w is the Warburg factor which is relative with Z', Rs is the resistance of the electrolyte and electrode material, Rct is the charge transfer resistance and ω is the angular frequency in the low frequency region. In order to get the Warburg factor (σ_w), the linear fitting of Z' in the low frequency region of these samples are shown in Fig. 7b. And the diffusion coefficient of sodium ion for these samples is listed in Table 2. It is quite clearly that the D_{Na+} of the NTP/C-P is higher than that of bare NTP. Meanwhile, it can also be found from the results that the NTP/C-F displays the lowest Rct and highest D_{Na+} value in accord with its good cyclic stability and outstanding electrochemical performance.

4. Conclusions

$NaTi_2(PO_4)_3$/C composite nanofibers (NTP/C-F) were synthesized via a simple electrospinning method and compared with bare $NaTi_2(PO_4)_3$ nanofibers (NTP) and $NaTi_2(PO_4)_3$/C composite particles (NTP/C-P). It has been demonstrated that NTP/C-F shows much better performance than bare NTP without carbon and NTP/C-P without 1D-structure. The NTP/C-F delivers a high discharge capacity of 130 mAh g^{-1} at 0.1C and presents outstanding rate capability, which shows discharge capacities as high as about 87 and 63 mAh g^{-1} at very high current densities of 10C and 20C, respectively. Besides, it displays satisfactory capacity retention at large rates. The discharge capacity remains as high as 93% of that in the first cycle after 500 cycles at 5C. Hence, the properties improve, attributing to its special 1D-structure with uniform electrically conductive carbon network. The detailed reasons are listed as follows: (1) short diffusion pathway is provided by the 1 D nanofibers; (2) its small nanosized NTP primary particles not only further favors fast transport of Na^+ and electrons to active material but also augment active sites for Na; (3) high electronic conductivity, which facilitate the charge transfer within the electrode and to the current collector, is provided by uniformly dispersive carbon. Furthermore, to avoid active material depart from the collector, the volume expansion during cycling is buffered by elastic carbon. Therefore, the $NaTi_2(PO_4)_3$/C composite nanofibers synthesized by our means are sodium-storage electrode materials with great promise for high-rate capability, long-cycle life-applications.

Acknowledgements

This study is financially supported by National Key Research and Development Program of China (2016YFA0201001), the National Natural Science Foundation of China (Grant No. 51672234), the Research Foundation of Education Bureau of Hunan Province (Grant No. 15B229), the Research Foundation for Hunan Youth Outstanding People from Hunan Provincial Science and Technology Department (2015RS4030), Hunan 2011 Collaborative Innovation Center of Chemical Engineering & Technology with Environmental Benignity and Effective Resource Utilization, and the Program for Innovative Research Cultivation Team in University of Ministry of Education of China (1337304).

Appendix A. Supplementary data

Supplementary data associated with this article can be found, in the online version, at http://dx.doi.org/10.1016/j.electacta.2017.09.020.

References

[1] R.C. Massé, E. Uchaker, G.Z. Cao, Sci. China Mater. 58 (2015) 715.
[2] Z.C. Yan, L. Liu, H.B. Shu, X.K. Yang, H. Wang, J.L. Tan, Q. Z, Z.F. Huang, X.Y. Wang, J. Power Sources 74 (2015) 8–14.
[3] Z.C. Yan, L. Liu, J.L. Tan, Q. Z, Z.F. Huang, D.D. Xia, H.B. Shu, X.K. Yang, X.Y. Wang, J. Power Sources 69 (2014) 37–45.
[4] P. Wang, D. Zhang, F. Ma, Y. Ou, Q.N. Chen, S. Xie, J. Li, Nanoscale 22 (2012) 7199–7204.
[5] Y. Ou, J. Wen, H. Xu, S. Xie, J. Li, J. Phys.Chem. Solids 74 (2013) 322–327.
[6] X. Li, X. Zhu, J. Liang, Z. Hou, Y. Wang, N. Lin, Y. Zhu, Y. Qian, J. Electrochem. Soc. 161 (2014) A1181–A1187.
[7] Y. Fang, L. Xiao, X. Ai, Y. Cao, H. Yang, Adv. Mater. 27 (2015) 5895.
[8] Z. Jian, W. Han, X. Lu, H. Yang, Y.-S. Hu, J. Zhou, Z. Zhou, J. Li, W. Chen, D. Chen, L. Chen, Adv. Energy Mater. 3 (2013) 156.
[9] Y. Fang, L. Xiao, J. Qian, X. Ai, H. Yang, Y. Cao, Nano Lett. 14 (2014) 3539.
[10] G. Pang, P. Nie, C. Yuan, L. Shen, X. Zhang, H. Li, C. Zhang, J. Mater. Chem. 25 (2016) 474–481.
[11] G. Pang, C. Yuan, P. Nie, B. Ding, J. Zhu, X. Zhang, Nanoscale 6 (2014) 6328–6334.
[12] B. Zhao, B. Lin, S. Zhang, C. Deng, Nanoscale 7 (2015) 18552–18560.
[13] S. Difi, I. Saadoune, M.T. Sougrati, R. Hakkou, K. Edstrom, P.E. Lippens, J. Phys. Chem. C 119 (2015) 25220–25234.
[14] Z. Huang, L. Liu, L. Yi, W. Xiao, M. Li, Q. Zhou, G. Guo, X. Chen, H. Shu, X. Yang, X. Wang, J. Power Sources 325 (2016) 474–481.
[15] L. Liu, T. Song, H. Han, H. Park, J. Xiang, Z. Liu, Y. Feng, U. Paik, J. Mater. Chem. A 3 (2015) 10395–10402.
[16] W. Wu, A. Mohamed, J.F. Whitacre, J. Electrochem. Soc. 160 (2013) A497–A504.
[17] J. Liu, J. Zhang, S. Cheng, Small 4 (2008) 1976–1979.
[18] X.Y. Wu, M.Y. Sun, Y.F. Shen, J.F. Qian, Y.L. Cao, X.P. Ai, H.X. Yang, ChemSusChem 7 (2014) 407–411.
[19] J. Yang, H. Wang, P.F. Hu, J.J. Qi, L. Guo, L.H. Wang, Small 11 (2015) 3721–3721.
[20] L. Wang, B. Wang, G.J. Liu, T.F. Liu, T.T. Gao, D.L. Wang, Rsc Advances 6 (2016) 74.
[21] G. Yang, H. Song, M. Wu, C. Wang, et al., J. Mater. Chem. A 3 (2015) 18718–18726.
[22] X. Li, X. Zhu, J. Liang, et al., J. Electrochem. Soc. 161 (2014) A1181–A1187.
[23] J. Song, S. Park, J. Gim, et al., J. Mater. Chem A 20 (2016) 7815–7822.
[24] C. Wu, P. Kopold, Y.L. Ding, Peter A.V. Aken, J. Maier, Y. Yu, Acs Nano 6 (2015) 6610–6618.
[25] D.A. Woodcock, P.J. Lightfoot, J. Mater. Chem. 9 (1999) 2907–2911.
[26] G. Yang, H. Song, M. Wu, C. Wang, et al., J. Mater. Chem. A 3 (2015) 18718–18726.
[27] D.A. Woodcock, Chem. Commun. 1 (1998) 107–108.
[28] D. Morgan, G. Ceder, M.Y. Saidi, J. Barker, J. Swoyer, H. Huang, G. Adamson, Chem. Mater 14 (2002) 4684–4693.
[29] Z.F. Huang, L. Liu, Q. Zhou, J.L. Tan, Z.C. Yan, D.D. Xia, H.B. Shu, X.K. Yang, X.Y. Wang, J. Power Sources 294 (2015) 650–657.
[30] Y.K. Zhou, B.L. He, W.J. Zhou, H.L. Li, J. Electrochem. Soc. 151 (2004) A1052–A1057.
[31] H.B. Shu, M.F. Chen, W. Fang, Y.Y. Fu, Q.Q. Liang, X.K. Yang, X.Y. W, Electrochim. Acta 152 (2015) 368–377.
[32] H. Qiu, H. Yue, T. Zhang, Y. Ju, Y. Zhang, Z. Guo, C. Wang, G. Chen, Y. Wei, D. Zhang, Electrochimica Acta. 188 (2016) 636–644.
[33] L.L. Zhang, S. Duan, X.L. Yang, G. Peng, G. Liang, Y.H. Huang, Y. Jiang, S.B. Ni, M. Li, ACS Appl. Mater. Interfaces 5 (2013) 12304–12309.